MEASUREMENT SCIENCE REVIEW, **17**, (2017), No. 6, 273-281

DE GRUYTER OPEN

MEASUREMENT SCIENCE REVIEW

Journal homepage: http://www.degruyter.com/view/j/msr

ISSN 1335-8871

The Enhancement of 3D Scans Depth Resolution Obtained by Confocal Scanning of Porous Materials

Dalibor Martisek, Jana Prochazkova

Institute of Materials Science and Engineering, NETME center, Brno University of Technology, Czech Republic, martisek@fme.vutbr.cz, prochazkova.j@fme.vutbr.cz

The 3D reconstruction of simple structured materials using a confocal microscope is widely used in many different areas including civil engineering. Nonetheless, scans of porous materials such as concrete or cement paste are highly problematic. The well-known problem of these scans is low depth resolution in comparison to the horizontal and vertical resolution. The degradation of the image depth resolution is caused by systematic errors and especially by different random events. Our method is focused on the elimination of such random events, mainly the additive noise. We use an averaging method based on the Lindeberg–Lévy theorem that improves the final depth resolution to a level comparable with horizontal and vertical resolution. Moreover, using the least square method, we also precisely determine the limit value of a depth resolution. Therefore, we can continuously evaluate the difference between current resolution and the optimal one. This substantially simplifies the scanning process because the operator can easily determine the required number of scans.

Keywords: Noise reduction, porous materials, confocal microscope, 3D scans, 3D reconstruction.

1. INTRODUCTION

The 3D reconstruction based on laser scanning confocal microscopy is an indispensable tool for civil engineering. Particularly in civil engineering, many different porous materials must be analysed. Common examples include the micro fractures in the concrete or the cement paste. However, the depth resolution of these scans is substantially influenced by additive noise and other disturbing factors. The described work is a result of cooperation between the Faculty of Civil Engineering and the Faculty of Mechanical Engineering, BUT that is focused on the precise evaluation of the concrete material properties.

In this article, we propose a method that eliminates the vast majority of the additive noise without degradation of useful information. This allows enhancing the depth resolution of the scans to the order comparable with horizontal and vertical resolution. Firstly, we describe the mathematical apparatus of our method. Subsequently, we assess our method with statistical evaluation and compare our results with methods used in common software tools that are provided with the microscopes.

2. SUBJECT & METHODS

2.1. Material and current methods

Our method follows on the recently published work on morphological analysis of fracture surfaces [2], [3] and also, porous materials in [1]. The gist of our work is the improvement of *z*-resolution that determines the quality of the reconstruction. The overview of common approaches used for 3D reconstruction can be found in [6], [9].

The *z*-resolution, i.e. optical sectioning thickness, depends on many factors: the wavelength of the used light, pinhole size, numerical aperture of the objective lens, refractive index of components in the light path, and the assembly of the instrument. The degradation of the *z*-resolution is often caused by systematic errors and by random events. Systematic errors, for example imperfections of the lens, light diffraction, are not random so that they cannot be detected and eliminated by existing methods that work only with random events. For example, the authors [5] use the weighted window function to reduce the Poisson noise in confocal scanning. Also, our previous article [7] describes the methods to eliminate noise. But the systematic errors are not random so these methods are not able to eliminate it.

Especially, additive noise is added to original values during the making, transfer or reproduction of an image.

In our work, we deal with the random events reduction, especially additive noise, to improve *z*-resolution.

During measurement, we scan the same point of the sample twice with the same conditions. In the case of noiseless measurements, we would get two identical results. Nevertheless, different values indicate the presence of noise. From the mathematical point of view, we consider everything what causes this difference as the noise (typically heat vibrations, also measurement errors, mechanical oscillations, etc.)

DOI: 10.1515/msr-2017-0034

Let us mention some methods for reducing additive noise – Richardson-Lusy algorithm (*RLA*), Maximum Likelihood Estimation (*MLE*), and Iterative Constrained Tikhonov-Miller (*ICTM*) algorithm [4]. However, these methods are limited by the additional assumptions, e.g. Poisson distribution of noise [5]. Low-pass filters are commonly used to reduce the additive noise as well [9]. The key purpose of these filters is the reduction of high spatial frequencies in the signal in the sense of the Fourier transform. Nevertheless, these filters are not able to differentiate whether the high-frequency information is caused by noise or by high contrast in the image. Therefore, loss of information necessarily ensues.

Our recent work [7] presents the method based on the Lindeberg-Lévy theorem as the pre-processing tool for single 2D images. In this paper, we introduce the application of this approach in confocal scanning to eliminate the random events (additive noise) and improve the *z*-resolution to the same values as the *xy*-resolution. We perform a statistical comparison of our results with the standard commercial software solution (Olympus software, version 6). The results are summarised in Section 3 and in Appendix, Table 4. and Table 5.

Table 4. shows that the average of seven or eight following measurements gives the results comparable with a low-pass filtered surface. The accuracy is higher with the increasing number of measurements and the correlation reaches the approximate value 0.999872 for K=25.

All sample measurements were made with confocal microscope Olympus LEXT OLS 3100. This microscope includes a confocal mode which collects the data to the Comma Separated Values (CSV) file with step 0.62 μm in the *z*-axis. This value may lead to the conviction that the measured surface has the same accuracy. Nevertheless, this confidence is quite false in the case of porous materials as is shown in Section 3. We use the confocal mode with the field of vision 2560× 1920 μm at a pixel resolution of 1024×768 pixels. It follows that the xy-resolution was 2.5 μm.

We work with the sample of fracture surface of hydrated Portland cement paste. For illustrative purposes, several specimens consisting of hydrated cement pastes were selected from a set of one-year old specimens. Ordinary Portland cement was used for their preparation. The specimens were mixed with the water-to-cement ratio equal to 0.4, and the fresh paste was cast in moulds of the size 2x2x10 cm^3. The paste was cured at a temperature of 20±2°C, and relative humidity of 100 % for three months. The specimens were then fractured in the three-point bending arrangement and sectioned into small cubes 2x2x2 cm^3. The rest of the time the cubes were stored under normal laboratory conditions (20±2 C, 101 325 kPa, 60±10 % RH).

2.2. Statistical evaluation

This section describes the statistical evaluation that is used in other sections to evaluate the results. We use these parameters: root mean square error, (relative) average difference, and Pearson's correlation coefficient.

Denote P, Q results of two different scans of the same profile, P_{ij}, Q_{ij} values of pixel $[i, j]$ in profiles P, Q, W, and H width and height of profile matrices of P, Q. Then the root mean square error is defined as:

$$RMSE = \sqrt{\frac{1}{W \cdot H}\sum_{i=1}^{W}\sum_{j=1}^{H}\left(P_{ij} - Q_{ij}\right)^2}$$

The average difference:

$$AD = \frac{1}{W \cdot H}\sum_{i=1}^{W}\sum_{j=1}^{H}\left|P_{ij} - Q_{ij}\right|$$

the relative average difference:

$$RAD = \frac{AD}{\Delta z} = \frac{1}{\Delta z}\cdot\frac{1}{W \cdot H}\sum_{i=1}^{W}\sum_{j=1}^{H}\left|P_{ij} - Q_{ij}\right|$$

where $\Delta z = 0.62\ \mu m$ is the used step in the z-axis. The value RAD indicates how many times the real accuracy is less than the step in the z-axis. Finally, Pearson's correlation coefficient

$$CORR = \frac{\sum_{i=1}^{W}\sum_{j=1}^{H}\left(P_{ij} - \bar{P}\right)\left(Q_{ij} - \bar{Q}\right)}{\sqrt{\sum_{i=1}^{W}\sum_{j=1}^{H}\left(P_{ij} - \bar{P}\right)^2 \sum_{i=1}^{W}\sum_{j=1}^{H}\left(Q_{ij} - \bar{Q}\right)^2}}$$

where $\bar{P},\ \bar{Q}$ are arithmetic means of profiles $P;\ Q$.

2.3. Noise decreasing method

Proposed noise reduction method is based on the Lindeberg-Lévy Central Limit Theorem, which produces more accurate results in comparison with low-pass filters and can be used without any limitations, unlike *RLA*, *MLE* or *ICTM*.

Consider the noise as the realization of a random variable. Then we can say:

Theorem (Lindeberg-Lévy Central Limit Theorem). *Let $X_1; X_2; \ldots; X_K$ be random variables with arbitrary (but the same) distribution, the same mean value μ and the same (finite) variance σ^2. Then the mean of $X_1; X_2; \ldots; X_K$ for $K \to \infty$ converges to the normal distribution with the same mean value μ and variance $\acute{\sigma}^2 = \sigma^2/K$.*

The proof of this theorem can be found in [8] for example. Generally, the application of the theorem causes that the mean variance of K random variables is K-times lower. This will be described further.

Let P be the input profile that consists of the useful information U and the noise N. The noise N is the realization of a random variable with expected values equal to zero. We carry out the profile measurements K-times, therefore we obtain the series $\{P(k)\}, k = 1, 2, \ldots, K$. Let U_{ij} be the useful information and $N_{ij}(k)$ be the random noise in pixel $[i, j]$ in

profile $P(k)$. The arithmetic means in $[i,j]$-th pixel can be expressed as:

$$\overline{P_{ij}(K)} = \frac{1}{K}\cdot\sum_{k=1}^{K} P_{ij}(k) = \frac{1}{K}\cdot\sum_{k=1}^{K}\left(U_{ij} + N_{ij}(k)\right) = U_{ij} + \frac{1}{K}\cdot\sum_{k=1}^{K} N_{ij}(k) \tag{1}$$

The useful information U_{ij} (it is not random) is preserved and noise is:

$$N_{ij} = \frac{1}{K}\cdot\sum_{k=1}^{K} N_{ij}(k) \tag{2}$$

Equation (2) denotes that the mean is equal to zero and the variance is K-times lower.

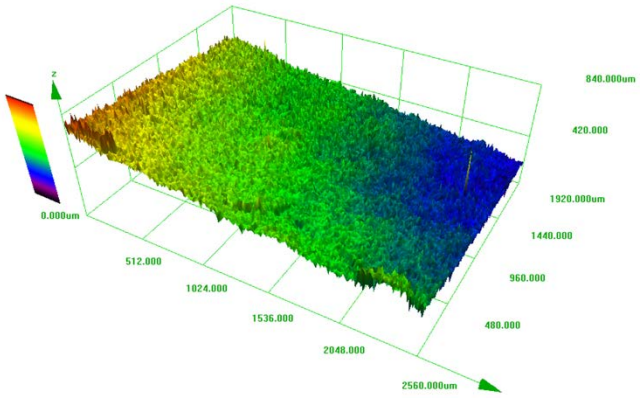

Fig.1. Non-filtered profile reconstructed with Olympus company software (step 0.62 μm in the *z*-axis) technology.

We use different statistical variables to compare our results. Let $\overline{P_{ij}(K)}$ be the arithmetic mean of K values in pixel $[i,j]$ in K scannings of the same profile. Let $\overline{Q_{ij}(K)}$ be the arithmetic mean of the following K values in pixel $[i,j]$ in the following K scannings of the same profile. Denote $RMSE(K)$, $AD(K)$; $RAD(K)$; $CORR(K)$ the root mean square error, average difference, relative average difference, and correlation of $\overline{P_{ij}(K)}$ and $\overline{Q_{ij}(K)}$, i.e.

$$RMSE(K) = \sqrt{\frac{1}{W\cdot H}\sum_{i=1}^{W}\sum_{j=1}^{H}\left(\overline{P_{ij}(K)} - \overline{Q_{ij}(K)}\right)^2}$$

where

$$\overline{P_{ij}(K)} = U_{ij}(K) + \frac{1}{K}\cdot\sum_{k=1}^{K} N_{ij}^{(P)}(k)$$

$$\overline{Q_{ij}(K)} = U_{ij}(K) + \frac{1}{K}\cdot\sum_{k=1}^{K} N_{ij}^{(Q)}(k)$$

It means

$$RMSE(K) = \frac{1}{K}\cdot\sqrt{\frac{1}{W\cdot H}\sum_{i=1}^{W}\sum_{j=1}^{H}\left(\sum_{k=1}^{K} N_{ij}^{(P)}(k) - \sum_{k=1}^{K} N_{ij}^{(Q)}(k)\right)^2} = \frac{1}{K}\cdot\sqrt{\frac{1}{W\cdot H}\sum_{i=1}^{W}\sum_{j=1}^{H}\left(\sum_{k=1}^{K}\left[N_{ij}^{(P)}(k) - N_{ij}^{(Q)}(k)\right]\right)^2} = \frac{1}{K}\cdot\sqrt{\frac{1}{W\cdot H}\sum_{i=1}^{W}\sum_{j=1}^{H}\left(\sum_{k=1}^{K} N_{ij}(k)\right)^2} \tag{3}$$

Similarly,

$$AD(K) = \frac{1}{K}\cdot\left[\frac{1}{W\cdot H}\sum_{i=1}^{W}\sum_{j=1}^{H}\left|\sum_{k=1}^{K} N_{ij}(k)\right|\right] \tag{4}$$

The expression $\sum_{k=1}^{K} N_{ij}(k)$ in (1), (2) describes the noise. Therefore, the expressions under the square root in (3) or whole expression in the square brackets (4) also determine the noise. This means that $RMSE(K)$ and $AD(K)$ are proportional to K inversely (where K denote the number of averaged scans).

Analogically, we can write:

$$RAD(K) = \frac{AD}{\Delta z} = \frac{1}{K}\cdot\frac{1}{\Delta z}\cdot\frac{1}{W\cdot H}\sum_{i=1}^{W}\sum_{j=1}^{H}\left|P_{ij}(K) - Q_{ij}(K)\right|$$

Correlation can be expressed as:

$$CORR(K) = \frac{\sum_{i=1}^{W}\sum_{j=1}^{H}\left(P_{ij}(K) - \overline{P(K)}\right)\left(Q_{ij}(K) - \overline{Q(K)}\right)}{\sqrt{\sum_{i=1}^{W}\sum_{j=1}^{H}\left(P_{ij}(K) - \overline{P(K)}\right)^2\sum_{i=1}^{W}\sum_{j=1}^{H}\left(Q_{ij}(K) - \overline{Q(K)}\right)^2}}$$

Note, that $0 < CORR,\ CORR < CORR(K), CORR(K) < 1$ and we can write $0 < CORR < CORR(K) < 1$.

3. Results and Discussion

As mentioned above, the Olympus LEXT OLS 3100 confocal microscope was used to acquire a CSV data file that describes the fracture surface of hydrated Portland cement paste (step 0.62 μm in the *z*-axis). For illustration, we show the surface reconstruction using Olympus company software in Fig.1. It confirms that reconstruction of porous materials is problematic and obviously, the image is also constructed with low resolution.

Fig.2. clearly shows that the reconstructed surface (by Olympus software) also contains a huge error. This error is clearly visible in Table 3. in Appendix where we compare the image section of two subsequent scans of the same area.

The differences covered the interval $-262\,\mu m$ to $+114\,\mu m$. Note that the z-step is $0.62\,\mu m$. For comparison,

we make the reconstruction of the same data using our proposed visualization software Micro3D.

We make five pairs $P^{(k)}; Q^{(k)}; \ k = 1, 2, \ldots, 5$ of same sample measurements. We compute the statistical characteristics $RMSE^{(k)}; \ AD^{(k)}; \ RAD^{(k)} \ CORR^{(k)}; \ k = 1, 2, \ldots, 5$ for each pair of these measurements. For each k, $P^{(k)}$ and $Q^{(k)}$ are measurements of the same profile, i.e. for each $k = 1, 2, \ldots, 5$ the ideal values are: $RMSE^{(k)} = 0;$ $AD^{(k)} = 0; RAD^{(k)} = 0\ \%; CORR^{(k)} = 100\ \%$. As we can see from Table 1., the average difference AD is approximately $23.5\ \mu m$, the measurement error is therefore approximately 38 times higher than the used step $0.62\ \mu m$. The correlation reaches the value 97 %.

Moreover, we filtered this data using Olympus company low-pass filter, and Table 2. presents the same characteristics as Table 1. The values of statistical parameters are significantly better. However, these filters are not able to differentiate whether the high-frequency information is a useful signal or the noise.

Therefore, low-pass filters decrease additive noise but also degrade the reconstructed surface. We can see this fact on the visualization. The surface reconstructed by Olympus Company software is presented in Fig.3. It is evident that low-pass filters are not suitable for porous materials because of the visible surface degradation.

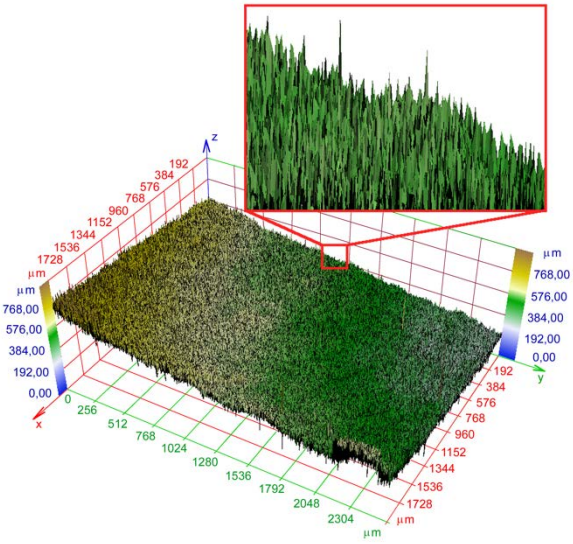

Fig.2. Non-filtered profile reconstructed with Micro3D software (same data as in Fig.1.)

Table 1. Comparison of five pairs of the same surface scans, non-filtered. (z-step 0.62 μm).

k	RMSE	AD	RAD	CORR
1	29.9229	23.4072	37.75	0.971787
2	29.944	23.4163	37.77	0.971762
3	29.9208	23.3903	37.73	0.971791
4	29.9884	23.4303	37.79	0.971667
5	30.0563	23.5059	37.91	0.971549

Table 2. The comparison of five pairs of the same surface scans filtered using Olympus company low-pass filter. (z-step 0.62 μm).

k	RMSE	AD	RAD	CORR
1	6.0940	4.5698	7.37	0.998676
2	6.1739	4.1664	6.72	0.998642
3	6.2504	4.6749	7.54	0.998610
4	6.3048	4.7052	7.59	0.998585
5	6.4391	4.7829	7.71	0.998529

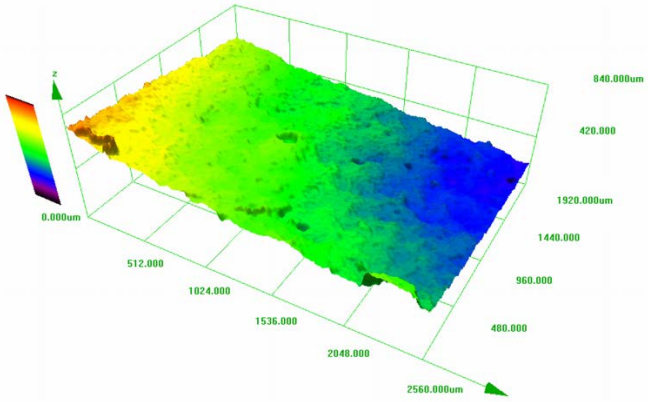

Fig.3. Profile from Fig.1. filtered by a common low-pass filter (Olympus company software).

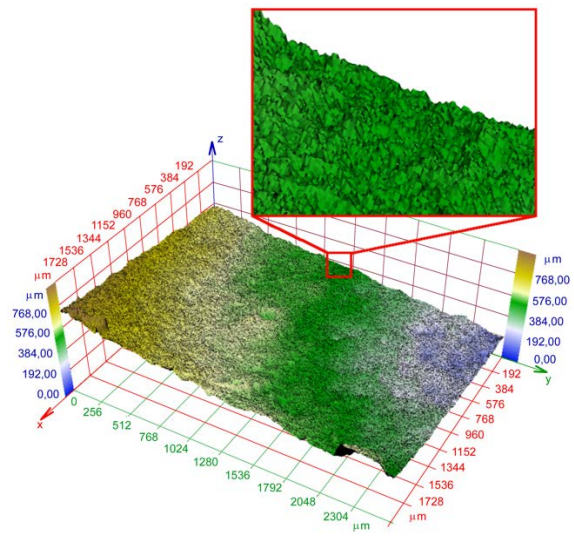

Fig.4. The surface composed of average values given by 25 scans - sample S_1 (Micro3D software).

The following part presents the advantage of the proposed noise reduction method using different statistical evaluation.

We make sequence of 25 pairs $P^{(k)}; Q^{(k)}; k = 1, 2, \ldots, 25$ of the sample S_1 measurements. Consequently, we calculated 25 pairs of averages of K profiles.

$$\overline{P(K)} = \frac{1}{K}\sum_{k=1}^{K} P^{(k)}; \qquad \overline{Q(K)} = \frac{1}{K}\sum_{k=1}^{K} Q^{(k)}; \qquad K = 1, 2, \ldots, 25 \tag{5}$$

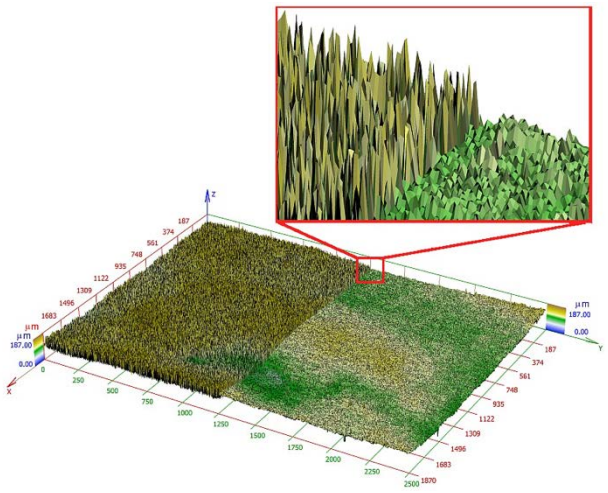

Fig.5. The surface composed of average values given by 25 scans - sample S_2 (Micro3D software).

For example, $\overline{P(10)}$ is the profile matrix calculated as the arithmetic mean of ten measurements $P^{(1)}$; $P^{(2)}$,..., $P^{(10)}$ of the same profile and $\overline{Q(10)}$ is the profile matrix calculated as the arithmetic mean of other ten measurements $Q^{(1)}$, $Q^{(2)}$,...;, $Q^{(10)}$ of the same profile. We compute the statistical characteristics between $\overline{P(K)}$ and $\overline{Q(K)}$ in dependence on the value of *K*.

Due to the Lindeberg-Lévy Central Limit Theorem, we eliminate the noise using (1), (2). Following computation of the statistical characteristics $RMSE(K)$, $AD(K)$, $RAD(K)$, and $CORR(K)$ between $\overline{P(K)}$ and $\overline{Q(K)}$ proves that the method improves the *z*-resolution significantly. The results in Table 4. show that the average of seven or eight following measurements *(K=7, 8)* gives the results comparable with a low-pass filtered surface. The accuracy is higher with the increasing number of measurements. The correlation reaches the approximate value 0.999872 for *K=25*. The surface composed of average values given by 25 scans is presented in Fig.4.

We make the measurement and the same computations as described in previous part for the second sample S_2 (profile of hydrated Portland cement paste). The analogy data to Table 4. are in Table 5., and the resulting surface is in Fig.5. (analogical to Fig.4.).

Due to the inverse proportion of $RMSE(K)$ and $AD(K)$ predicted in Section 2., measured data was fitted with a function $f(K) = \frac{a}{K} + b$ by the least squares method.

We obtain for the first sample data these equations:

$$RMSE(K) = \frac{a}{K} + b \approx \frac{27{,}32}{K} + 2.63 \tag{6}$$

$$AD(K) = \frac{c}{K} + d \approx \frac{22{,}15}{K} + 1.82 \tag{7}$$

The functions (6) and (7) are drawn in Fig.6. The noise variance gives the numerators in these equations. The additive constant *d* in (7) describes the difference from a supposed inverse proportion. This difference is probably caused by some non-random measurement error of the microscope. The additive constant depicts that even in the case of perfect additive noise reduction ($K \to \infty$) it is not possible to reconstruct the profile exactly. The limit precision is $\pm\frac{d}{2} \approx \pm 0{,}9\ \mu m$.

The sample S_2 values of a, b, c, d in (6), (7) are equal to $a = 27.04$; $b = 2.78$; $c = 21.92$; $d = 2.06$ and corresponding functions are in Fig.7.

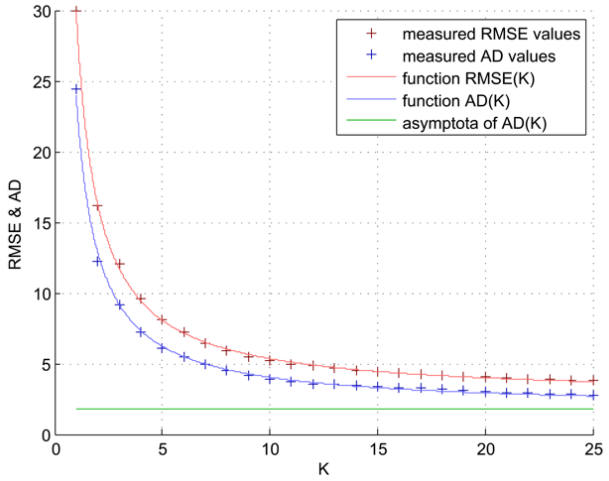

Fig.6. Functions *RMSE* and *AD* for sample S_1 – reliance of Root Mean Square Error and Average Difference on the number of averaged scans.

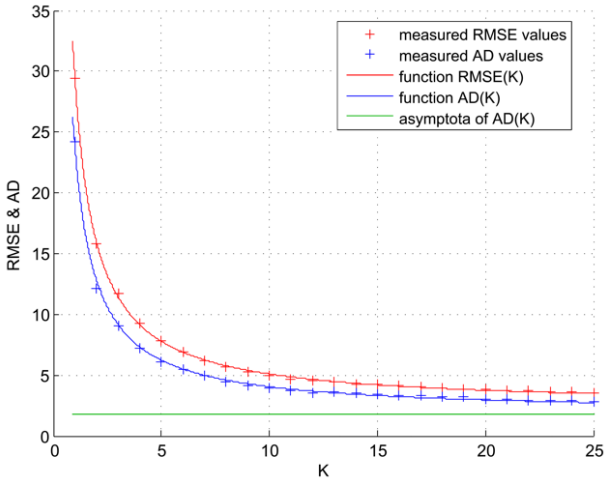

Fig.7. Functions *RMSE* and *AD* for sample S_1 – reliance of Root Mean Square Error and Average Difference on the number of averaged scans.

4. CONCLUSIONS

We have used the field of vision 2560× 1920 μm, a pixel resolution of 1024×768 pixels so that the xy-resolution was 2.5 μm. In our case, the z-resolution of input data was 0.62 μm. The course of the function $AD(K)$ indicates that we can improve the resolution even with low-quality data using 4-6 subsequent scans. The usage of 25 scans causes the improvement of z-axis resolution on the level comparable to the xy-resolution. Theoretically, due to additive constant d, maximal additive noise reduction ($K \to \infty$) means that the maximal resolution for tested samples is $\pm\frac{d}{2} \approx \pm 0.9\ \mu m$, and $\pm\frac{d}{2} \approx \pm 1.0\ \mu m$, i.e. three and 2.5 times higher resolution in comparison with xy-resolution. This method based on the Lindeberg–Lévy theorem is able to set the optimal number of measurements to get the required depth precision.

ACKNOWLEDGMENT

The authors acknowledge support from Project LO1202 by financial means from the Ministry of Education, Youth and Sports, the National Sustainability Programme I. The authors thank prof. Tomas Ficker from the Faculty of Civil Engineering of Brno University of Technology for the provided data.

REFERENCES

[1] Ficker, T., Len, A., Chmelík, R., Lovicar, L., Martišek, D., Němec, P. (2007). Fracture surfaces of porous materials. *Europhysics Letters*, 80 (6), 1600-1604.

[2] Ficker, T., Martišek, D., Jennings, H.M. (2010). Roughness of fracture surfaces and compressive strength of hydrated cement pastes. *Cement and Concrete Research*, 40 (6), 947-955.

[3] Ficker, T., Martišek, D. (2012). Digital fracture surfaces and their roughness analysis: Applications to cement-based materials. *Cement and Concrete Research*, 42 (6), 827-833.

[4] Van Kempen, G.M.P., Van Vliet, L.J., Verveer, P.J., Van Der Voort, H.T.M. (1997). A quantitative comparison of image restoration methods for confocal microscopy. *Journal of Microscopy*, 185, 354-365.

[5] Kervrann, C., Trubuil, A. (2004). An adaptive window approach for Poisson noise reduction and structure preserving in confocal microscopy. In *2nd IEEE International Symposium on Biomedical Imaging: Nano to Macro*, Arlington, VA, USA. IEEE, 788-791.

[6] Sheppard C.J.R., Shotton D.M. (1997) *Confocal Laser Scanning Microscopy*. Springer.

[7] Martisek, D., Prochazkova, J., Ficker, T. (2015). High-quality three-dimensional reconstruction and noise reduction of multifocal images from oversized samples. *Journal of Electronic Engineering*, 24 (5).

[8] Montgomery, D.C., Runger, G.C. (2003). *Applied Statistics and Probability for Engineers*, 3rd ed. John Wiley & Sons.

[9] Yio, M.H.N., Mac, M.J., Wong, H.S., Buenfeld, N.R. (2015). 3D imaging of cement-based materials at submicron resolution by combining laser scanning confocal microscopy with serial sectioning. *Journal of Microscopy*, 258 (2), 151-169.

Received May 19, 2017.
Accepted November 13, 2017.

APPENDIX

Table 3. Two submatrices of heights of the same sample points acquired by two subsequent scans (z-step 0.62 μm) and their differences (all in micrometers).

First scanning

542.85	562.70	556.07	566.79	553.22	545.08	274.90	554.55	576.03	506.31	518.87	523.18	556.51
538.57	568.27	560.31	576.65	509.64	516.04	526.16	550.84	543.13	596.15	539.87	570.22	588.08
588.11	570.42	559.23	558.35	572.98	563.72	541.97	571.48	550.09	492.95	551.80	555.34	571.24
560.49	577.91	599.61	573.03	586.78	564.28	563.84	587.45	554.41	577.02	577.18	559.52	554.95
563.75	559.75	624.12	573.59	552.75	521.04	531.06	601.79	574.48	571.30	560.83	560.34	585.82
552.68	540.69	547.04	563.95	552.87	558.38	568.50	549.32	539.15	559.13	559.33	557.79	536.69
567.29	580.02	569.31	569.65	553.17	538.72	489.03	519.95	544.29	570.86	573.38	554.37	569.80

Second scanning

580.01	531.17	580.64	529.34	545.78	539.43	536.89	603.34	537.14	554.97	548.45	565.95	555.79
555.20	557.44	556.71	574.78	559.01	571.09	564.41	560.34	582.43	572.75	507.05	538.50	544.71
519.34	548.63	552.61	559.06	567.07	584.37	559.08	557.77	554.29	569.76	538.78	557.55	542.16
531.10	577.58	529.96	550.27	575.13	568.18	552.65	533.79	537.70	548.60	566.12	488.60	508.98
568.32	558.87	510.08	563.84	566.87	573.43	564.06	517.01	514.14	586.94	542.68	515.10	529.12
545.59	570.74	582.44	581.88	559.33	537.92	565.95	564.70	557.55	580.76	555.95	487.07	561.33
576.52	564.66	545.22	581.80	525.63	576.65	577.54	563.64	546.92	541.52	529.59	568.95	581.74

Differences

-37.16	31.53	-24.57	37.45	7.45	5.64	**-261.98**	-48.79	38.89	-48.66	-29.58	-42.77	0.73
-16.63	10.84	3.60	1.86	-49.36	-55.05	-38.25	-9.49	-39.30	23.39	32.82	31.72	43.37
68.77	21.78	6.62	-0.71	5.91	-20.65	-17.11	13.71	-4.20	-76.80	13.02	-2.21	29.08
29.39	0.32	69.65	22.76	11.65	-3.89	11.19	53.66	16.72	28.42	11.06	70.92	45.96
-4.56	0.88	**114.04**	9.76	-14.13	-52.39	-33.00	84.78	60.34	-15.64	18.14	45.23	56.70
7.08	-30.04	-35.41	-17.93	-6.45	20.45	2.55	-15.39	-18.40	-21.63	3.37	70.71	-24.64
-9.23	15.36	24.09	-12.15	27.54	-37.93	-88.51	-43.69	-2.63	29.34	43.79	-14.57	-11.94

Table 4. Comparison of twenty-five pairs of the same surface measurements. Each measurement in each pair is the average of $K = 1, 2\ldots, 25$ scannings (Sample S_1).

K	RMSE(K)	AD(K)	RAD(K)	CORR(K)
1	29.9206	24.3918	39.34	0.976197
2	16.1997	12.2270	19.72	0.991638
3	12.0631	9.1397	14.74	0.995344
4	9.5787	7.2473	11.69	0.997058
5	8.0759	6.0922	9.83	0.997907
6	7.2181	5.4557	8.80	0.998326
7	6.4875	4.9875	8.04	0.998647
8	5.9424	4.4872	7.24	0.998864
9	5.4966	4.1483	6.69	0.999028
10	5.2196	3.8716	6.24	0.999156
11	4.9286	3.7250	6.01	0.999260
12	4.8247	3.5197	5.68	0.999340
13	4.7255	3.5833	5.78	0.999422
14	4.4789	3.4893	5.63	0.999498
15	4.4706	3.4192	5.51	0.999562
16	4.3470	3.3203	5.36	0.999604
17	4.2757	3.2708	5.28	0.999649
18	4.1745	3.1889	5.14	0.999682
19	4.1218	3.1536	5.09	0.999715
20	4.0364	3.0038	4.84	0.999749
21	3.9972	2.9587	4.77	0.999783
22	3.9334	2.9078	4.69	0.999806
23	3.8863	2.8604	4.61	0.999828
24	3.8373	2.8461	4.59	0.999851
25	3.7989	2.8046	4.52	0.999872

Table 5. Comparison of twenty-five pairs of the same surface measurements. Each measurement in each pair is the average of $K = 1, 2\ldots, 25$ scannings (Sample S_2).

K	RMSE(K)	AD(K)	RAD(K)	CORR(K)
1	29.4196	24.2045	39.65	0.976385
2	15.8359	12.1613	19.83	0.991685
3	11.7407	9.1049	14.80	0.995363
4	9.2811	7.2314	11.72	0.997066
5	7.7933	6.0879	9.84	0.997909
6	6.9441	5.4578	8.80	0.998326
7	6.2208	4.9942	8.03	0.998645
8	5.6812	4.4989	7.23	0.998862
9	5.2398	4.1634	6.67	0.999025
10	4.9656	3.8895	6.22	0.999153
11	4.6775	3.7444	5.98	0.999256
12	4.5746	3.5411	5.65	0.999337
13	4.4764	3.6041	5.75	0.999419
14	4.2323	3.5110	5.60	0.999495
15	4.2241	3.4416	5.48	0.999560
16	4.1017	3.3437	5.33	0.999602
17	4.0311	3.2947	5.25	0.999647
18	3.9309	3.2136	5.11	0.999680
19	3.8788	3.1787	5.05	0.999713
20	3.7942	3.0304	4.80	0.999747
21	3.7554	2.9857	4.73	0.999781
22	3.6923	2.9353	4.65	0.999804
23	3.6456	2.8884	4.57	0.999827
24	3.5971	2.8743	4.55	0.999850
25	3.5591	2.8332	4.48	0.999871